Abburi Venkata, K., Truman, C. E., Wimpory, R. C., & Pirling, T. (2018). Numerical simulation of a three-pass TIG welding using finite element method with validation from measurements. *International Journal of Pressure Vessels and Piping*, *164*, 68-79. https://doi.org/10.1016/j.ijpvp.2017.05.014

Numerical simulation of a three-pass TIG welding using finite element method with validation from measurements

K. Abburi Venkata[a]*, C.E. Truman[a], R.C. Wimpory[b], T. Pirling[c]

[a]*University of Bristol, Solid Mechanics Research Group, Department of Mechanical Engineering, Bristol, BS81TR, UK*
[b]*Helmholtz-Zentrum Berlin, Department of Microstructure and Residual Stress Analysis, Berlin, 14109, Germany*
[c]*The Institut Laue-Langevin, Diffraction Group (DIF), Grenoble, 38042, France*

Abstract

Structural integrity assessment of welded joints requires characterising the residual stresses generated during the process. Although measurements can provide a quantitative estimation of the residual stresses, a reliable numerical model offers greater advantages in terms of cost, time and versatility. A validated model can be used to optimise the measurement procedure and thereby aiding in further refinement of the model itself. In the current work, a three-pass tungsten-inert gas welding in an austenitic stainless-steel plate is simulated using a three-dimensional sequentially coupled thermo-mechanical analysis for the purpose of predicting the transient thermal profiles and the final residual stresses as a part of NeT programme. Block-dumped heat transfer analysis was conducted with element activation and deactivation to represent the physical deposition of the weld beads for each pass, followed by a mechanical analysis to predict the stresses. Incremental deep-hole drilling and neutron diffraction techniques at ILL and HZB facilities in Grenoble and Berlin respectively, were employed to measure the residual stresses through the thickness of the sample plate at the centre. The predicted thermal history and the residual stresses are verified with the measured thermocouple recordings and the stresses respectively.

Keywords: Three-pass weld; TIG welding; neutron diffraction; finite element analysis; hole-drilling; element activation and deactivation.

1. Introduction

The European Network on Neutron Techniques Standardization for Structural Integrity (NeT) was established in 2002 to develop experimental and numerical techniques and standards for reliable characterisation of residual stresses in structural welds [1]. It involves partners from 35 organisations ranging from industrial, academic and research facilities from countries in Europe and beyond. Each problem is undertaken through round robins on measurement and modelling activities and subsequent interpretation of results by a dedicated Task Group (TG). Task Group 4 was established in 2007 to develop a three-pass slot weld benchmark made from Type 316L stainless steel. The specimen geometry is selected such that it is representative of weld repairs employed in engineering applications. The multi-pass welding serves as an increase in complexity over single-pass welds (TG1) through the generation of a complex 3D residual stress distribution.

The TG4 has launched parallel measurements and simulation round robins for comparison and standardisation of measurement and simulation protocols for residual stress characterising in complex weldments. As a part of the round robin research, 3D finite element (FE) simulation using ABAQUS v6.12 code was conducted to predict residual stresses from the welding process along with measurements using incremental deep hole drilling and neutron diffraction techniques on the sample weldment to characterise residual stresses. The predicted transient thermal profile and the residual stresses were compared with the measured values in order to validate the FE model and predictions. Apart from this, the results from the FE model and measurements were used in round robin comparisons with predictions and measurements from other partners in the TG [2, 3]. The current paper presents the details about the samples including preparation, various batches, welding process, the numerical modelling and measurement procedures on samples from various batches and discusses the results from predictions and measurements, drawing conclusions.

* Corresponding author
E-mail address: k.abburivenkata@bristol.ac.uk (Kiranmayi Abburi Venkata)

2. Sample details

The NeTTG4 specimen was a 3-pass slot weld in AISI 316L austenitic steel, made using the TIG welding process [1, 4]. The dimensions of the plate were 194 mm x 150 mm x 18 mm, while the slot was 80 mm long and 6 mm deep. Twelve identical specimens with slots were machined from a large blank of 316L stainless steel. Ten of the twelve specimens were set aside for characterization purposes including creation of weld macrographs, specimen destruction for contour method and deep hole drilling measurements. The remaining two were used for trial welding and fine tuning of welding parameters. Out of the ten specimens, one plate was set aside for manufacturing the weld pad. The remaining nine plates had slots machined in them. The schematic of the plate with the slot dimensions is given in Fig. 1. The plates were then subjected to solution heat treatment, to reduce any residual stresses introduced through machining, by heating up to 1050 °C at a rate of 5 °C min^{-1}, holding at this temperature for 45 min, cooled down in the furnace up to 300 °C and then air cooled to room temperature.

From the nine plates, one was reserved to characterise any residual stresses in the plates prior to welding. Another plate was reserved for thermocouple instrumentation at the University of South Brittany leaving seven plates for to be welded. Prior to welding, five thermocouples were spot-welded to the welded side mid-length position of the weld, but offset from the weld centreline. The thermocouple locations are shown in Fig. 2. This was done for two specimens. On the third specimen both strain gauges and thermocouples were applied as shown in the back face in Fig. 2. The remaining four specimens had no special instrumentation applied. The reason for seven plates was to circulate four plates for neutron and synchrotron X-ray diffraction based round robin residual stress measurements and two specimens for destructive stress measurement methods such as contour method, slitting and hole drilling, leaving one specimen for detailed metallography and extraction of d_0 specimens.

The plates were TIG welded using argon as the shielding gas and had an approximate heat input of 1.5 to 1.8 $kJmm^{-1}$. The welding was performed at Rolls Royce, Derby. Three weld passes were made into the slot, with each pass depositing the filler material directly on top of the predecessor, to fill the slot. The specimens were lightly clamped in a vice. The travel speed was 76.2 mm min^{-1}. The inter-pass temperatures for pass 2 and pass 3 are about 50 to 60 °C. The filler wire used was AWS A5.9-93 (ER316L) with a diameter of 0.9 mm. The chemical composition of the filler material is tabulated in Table 1. A tungsten electrode of approximately 3.2 mm in diameter was used in the welding process. The specimen fabrication, preparation and subsequent welding was performed strictly adhering to the manufacturing protocol written specifically for the TG4 problem [4].

Later an additional batch of six specimens were manufactured by TWI, Cambridge, for further characterisation including repeated contour and slitting measurements, additional neutron diffraction and over-core strain relief measurement. The additional six samples were notionally identical to the first set of twelve samples in the sense that the sample preparation prior to the welding process and the actual welding parameters were maintained the same. However, there were slight variations in the welding pass lengths and the measures implemented to overcome the underfill at the weld start end.

Table 1. Chemical composition of the base plate made of AISI Type 316L stainless steel (%wt.)

Element	C	Mn	Si	P	S	Cr	Ni	Mo	Cu
316L	0.03	2.0	0.5	0.025	0.01	18.0	12.5	2.70	0.3

3. Incremental deep hole drilling experiment

Incremental deep hole drilling method (iDHD) was used to measure the residual stresses arising from the three-pass welding on the TG4 sample manufactured by Rolls Royce, Derby i.e., from the first batch. The experiment was conducted in the residual stress lab at the University of Bristol. The measurements were made through the thickness of the specimen at the center of the weld. The schematic of the hole drilling technique is shown in Fig.3. The photograph of the plate measured is shown in Fig. 4. The various lines used for measurement and prediction of residual

stresses on the specimen are indicated in the schematic shown in Fig.5. The stresses were measured in the transverse (xx) and longitudinal (zz) directions and the in-plane shear stress (zx) along the line BD as shown in Fig. 5.

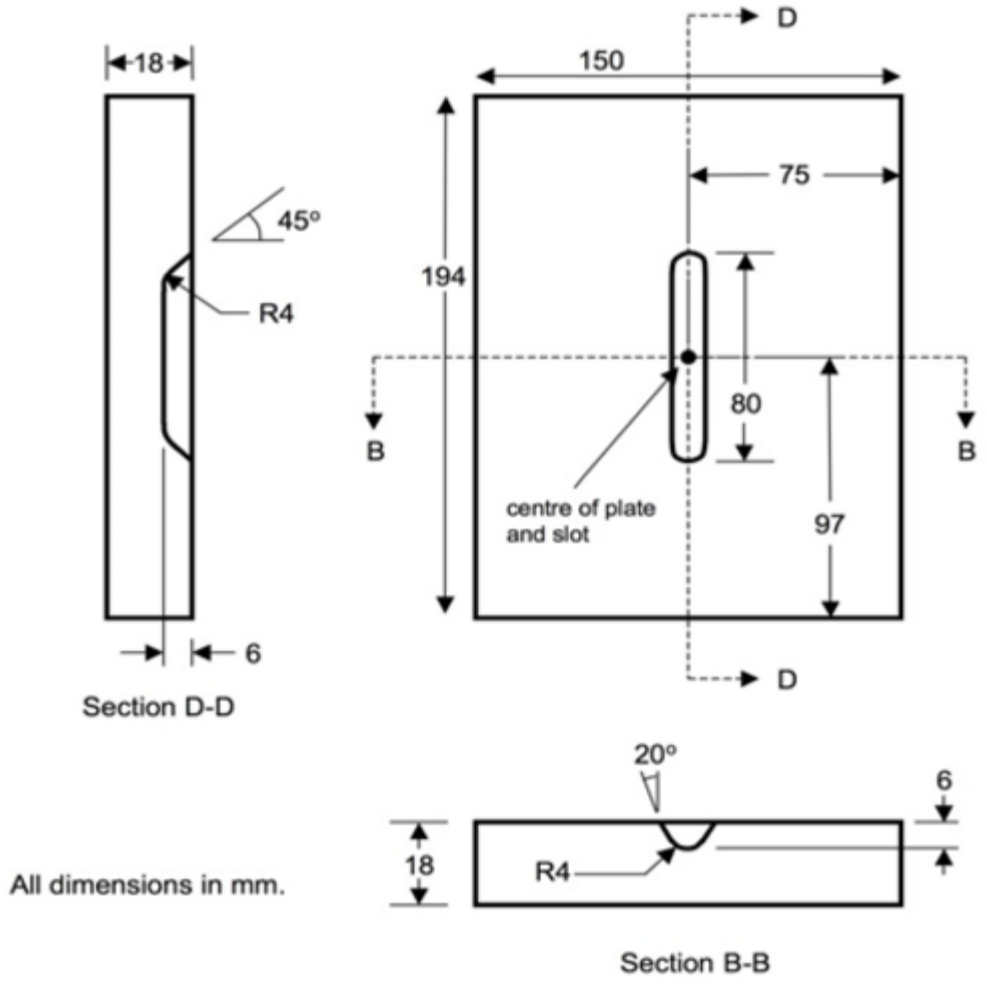

Fig. 1. Schematic representation of TG4 sample [1, 4]

The center of the specimen also coincident with the center of the weld was marked precisely on the sample. A front bush and a back bush were attached on the top and bottom faces of the sample such that they were coincident with the center of the sample. A reference hole of 1:5mm was drilled using a gun drilling process. The diameter of the reference hole was measured at eight different angles at a depth increment of 0:2mm through the whole thickness of the plate. After measuring the initial diameter of the reference hole, incremental trepanning was carried out using EDM process to measure the change in the diameter of the reference hole due to strain release. The core was trepanned in total increments of 17, through the thickness of the plate, to avoid the influence of plasticity release, which might affect the accuracy of the measurements. At each increment, the diameter of the reference hole was remeasured for every 0:2mm through the depth, at 8 different angles. The measured values of the diameters at all different angles were analysed using a bespoke application developed by VEQTER Ltd, Bristol.

The expression for the calculation of strain from the diameters of the reference hole measured is given as [5, 6, 8, 9]

$$V_{rr} = \frac{(d_{aEDM} - d_{bEDM})}{d_{bEDM}} \quad (1)$$

where V_{rr} is the radial distortion matrix, d_{aEDM} and d_{bEDM} are the diameters of the reference hole after and before trepanning respectively. The strains were calculated at each increment in all the angles. The calculated strains were then used to determine the in-plane residual stresses namely longitudinal (zz) and transverse (xx) and in-plane shear stress (zx).

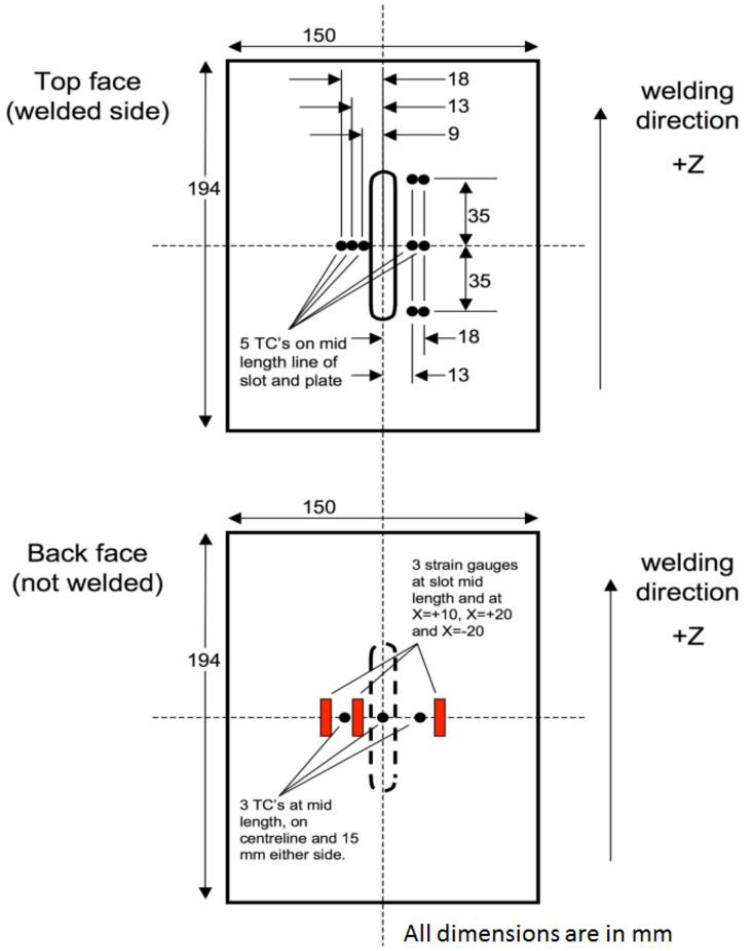

Fig. 2. Schematic of the thermocouple location on the TG4 sample [1, 4]

The stresses were determined using the relation

$$[V_{rr}] = -\frac{1}{E}[A]\sigma \quad (2)$$

where $[V_{rr}]$ is the distortion matrix in the radial direction, E is the Young's modulus assumed as 195.6 GPa for the parent material and 171 GPa for the weld material [10], σ is the in-plane stress matrix and $[A]$ is a pseudo matrix [11].

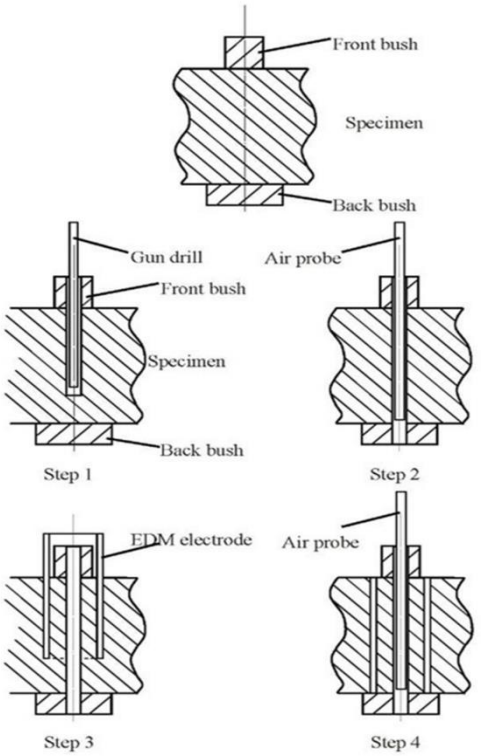

Fig. 3. A representation of the steps in standard DHD technique: step 1: reference hole generation; step 2: reference hole measurement; step 3: trepan the core and step 4: reference hole re-measured [5, 6]

The matrices can be expanded as,

$$\bar{V}_{rr} = \begin{bmatrix} \bar{V}_{rr}(\phi_1) \\ \bar{V}_{rr}(\phi_2) \\ \vdots \\ \bar{V}_{rr}(\phi_N) \end{bmatrix} \qquad A = \begin{bmatrix} a(\phi)_1 & b(\phi)_1 & c(\phi)_1 \\ a(\phi)_2 & b(\phi)_2 & c(\phi)_2 \\ \vdots & \vdots & \vdots \\ a(\phi)_N & b(\phi)_N & c(\phi)_N \end{bmatrix} \qquad \sigma = \begin{bmatrix} \sigma_{xx} \\ \sigma_{yy} \\ \sigma_{xy} \end{bmatrix} \tag{3}$$

where σ_{xx}, σ_{yy} are the normal stresses and σ_{xy} is the shear stress in plane. The functions $a(\phi)$, $b(\phi)$and $c(\phi)$are given as [6, 8]

$$f(\phi) = 1 + \cos 2\phi \tag{4}$$

$$g(\phi) = 1 - 2\sin\phi \tag{5}$$

$$h(\phi) = 4\sin(2\phi) \tag{6}$$

From Eq. (2), the values of stress are calculated using the equation [6, 8],

$$\sigma = -EA^*\bar{V}_{rr} \tag{7}$$

where

$$-E\bar{V}_{rr} = \varepsilon \tag{8}$$

Hence Eq. (7) can be re-written as,

$$\sigma = A^*\varepsilon \tag{9}$$

where A^* is the pseudo-inverse of [A] and is expressed as

$$A^* = (A^T A^{-1})A^T \tag{10}$$

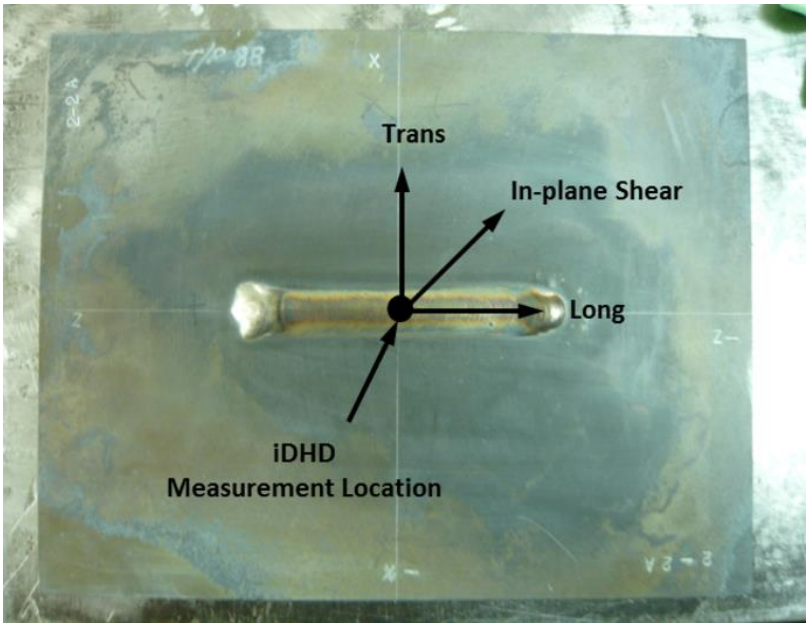

Fig. 4. Photograph of the sample used for iDHD measurement with measurement location

4. Neutron diffraction experiment at ILL

Subsequent to the hole-drilling experiments, residual stresses in the TG4 sample from batch one was measured using the non-destructive neutron diffraction technique on the strain diffractometer SALSA, at ILL facility in Grenoble, France. The measurements were made along the lines D2, B2 and BD indicated in Fig. 5. The drill down measurement along line BD has top priority for validating numerical simulations as it passes through all three weld passes and parent material under the weld beads. Line D2 is estimated to cover the last weld bead. Line B2 cuts perpendicularly through the weld line in order to provide steep stress gradients across various zones (fusion zone, HAZ and parent). Considering the sample geometry and symmetry conditions, the direction of the principal strains was assumed to coincide with those of the welding stresses. The strains were measured in all the principal strain directions.

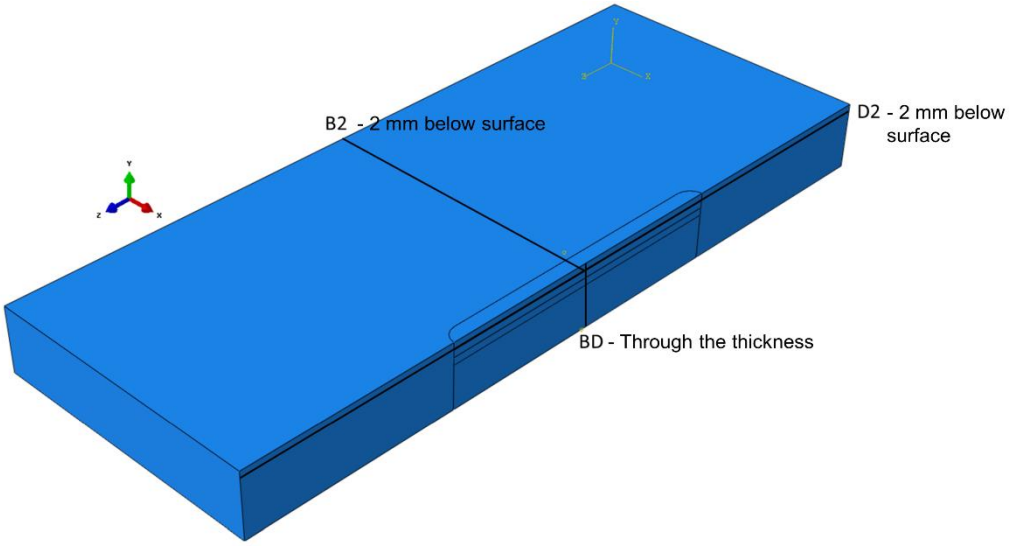

Fig. 5. Lines of measurement and predictions on the half model of the TG4 sample [7]

A gauge volume of 3 mm x 3 mm x 3 mm was employed during the measurements through the aid of slits. In order to measure the stress-free lattice spacing, three strain free cuboids with the dimensions 5 mm x 8 mm x 6 mm were fabricated by adhesively bonding together four small cuboids with dimensions 5 mm x 4 mm x 3 mm. The dimensions of the subcuboids relate to the dimensions of the plate to recover their orientation with respect to the plate [1, 4]. d_0 cubes were extracted from three different locations of the sample corresponding to the weld top and root and parent regions. The schematic of the reference specimens and the measurement grid is shown in Fig. 6.

Measurements of the lattice parameter were made considering the reflections from the (311) plane, as this plane is supposed to be unaffected by the presence of any inter-granular strains, thereby providing a reliable measure of macro residual strains [10, 12]. In order to get reflections from both the front face (top face) as well as the back face (bottom face) along the line BD, the measurements through the thickness (line BD) were repeated by rotating the specimen by 180° with respect to the first measurement position. This was done to check if there are any effects of texture or grain size. Welding often alters the microstructure of the material that can sometimes produce rapid texture gradients. These can be a source of systematic errors in neutron diffraction [13]. Therefore, reflections were taken from front face as well as back face by rotating the specimen by 180°.

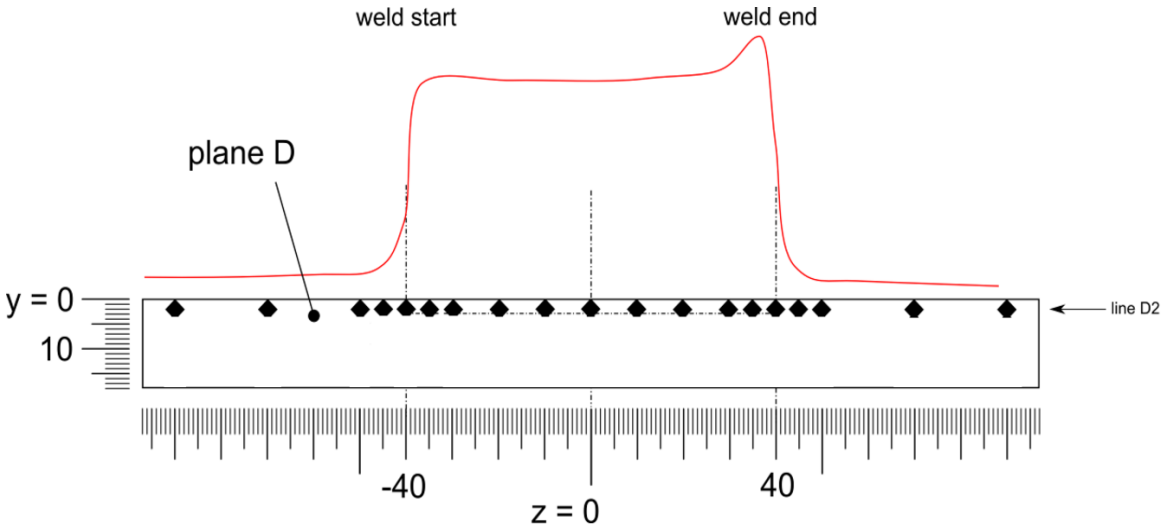

(a) Measurement grid along D2

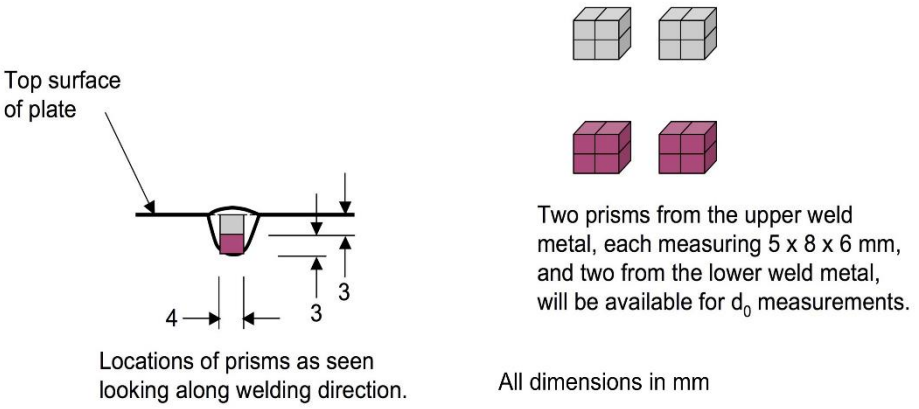

(b) Schematic of d_0

Fig. 6. Schematic of the measurement grid and d_0 specimen preparation for neutron diffraction

The measured lattice spacing was analysed using LAMP software by fitting the parameters such as the height, width of the diffraction peak and the background considering the full width half maximum height of the diffraction peak (FWHM), with a Gaussian distribution. As SALSA uses a monochromatic radiation with a fixed wavelength, the elastic strains were calculated from the relation Eq. (11) [10, 14]

$$\varepsilon_{xx} = \frac{\sin(\theta_{0x})}{\sin(\theta_x)} - 1 \tag{11}$$

where θ_{0x} and θ_x are the diffraction peak positions in the stress-free and stressed samples, ε_{xx} is the strain in *x*-direction. The stress was calculated using Eq. (13)

$$\sigma_{xx} = \frac{E}{(1+\nu)}\left[\varepsilon_{xx} + \frac{\nu}{(1-2\nu)}(\varepsilon_{xx} + \varepsilon_{yy} + \varepsilon_{zz})\right] \tag{12}$$

where σ_{xx} is the stress in the *x*-direction, E is the Young's modulus taken as 183.6 GPa and ν is the Poisson's ratio assumed as 0.3 [1].

5. Neutron diffraction experiment at HZB

Owing to the unusually higher magnitude of normal stresses (yy) measured along the line BD on strain diffractometer SALSA, further measurement of residual stresses was undertaken. Another neutron diffraction experiment was conducted on the TG4 specimen from batch two using the strain diffractometer E3, at HZB facility in Berlin, Germany. Considering the sample geometry and symmetry conditions, the direction of the principal strains was assumed to coincide with those of the welding stresses. The strains were measured in all the principal strain directions. The lattice parameters were measured for all the principal stress directions. The lattice spacing was measured for the (311) plane [10, 12]. The d_0 cuboid samples were extracted exactly at the same locations corresponding to those from batch one, i.e., from the weld top and root and parent locations. A transverse section of 5 mm was extracted from the mid-section of one of the sample plates using electron discharge machining (EDM). Two cuboid samples measuring 5 mm x 4 mm x 3mm were machined from the weld top and root regions. Another cuboid of same dimensions was extracted from the regions corresponding to the parent material.

A gauge volume of 3 mm x 3 mm x 2 mm was employed while measuring the lattice spacing. The measurements were made along the lines D2, B2 and BD as shown in Fig. 5. The measurement points along D2 and B2 were 10 mm apart and on the line BD were 2 mm apart. The measured lattice spacing was analysed using CARESS software by fitting the parameters such as the height, width of the diffraction peak and the background considering the full width half maximum height of the diffraction peak (FWHM), with a Gaussian distribution. The residual strains and stresses were calculated from the measured lattice spacing using the equations described in Eq. (11) and Eq. (13) respectively.

6. Finite element analysis

To predict the residual stresses arising from the multiple weld passes, a finite element analysis with sequentially coupled thermal and mechanical analysis was conducted using ABAQUS v6.12 code. The mesh of the half model of the sample is shown in Fig. 7. To make use of the symmetry of the plate, only a half of the plate along the weld line was modelled in the analysis. The number of nodes and elements in the mesh were 142970 and 134344 respectively. The element size in the weld was 0.9 mm x 0.75 mm x 0.35 mm. First order hexahedral, heat transfer elements and 3D stress elements were used in the thermal and mechanical analysis respectively. First order elements were used to reduce computation time.

Two popular methods known as block-dumped and moving heat source are employed widely to simulate the application of welding torch. For relative ease of application, the thermal analysis was conducted using block-dumped approach with ABAQUS v6.12 code [15] in which the weld beads are combined and deposited simultaneously. The volumetric heat flux needed to heat the elements was calculated using the welding power, torch speed and the weld mesh size. The initial temperature of the sample was set to 20 °C. The heat loss to the surroundings was modelled using convection and radiation. The convective heat transfer coefficient was assumed to be 7 W/m^{2}K. The radiation emissivity was considered as 0.8. Both the convective heat transfer coefficient and the radiation emissivity were

assumed to be independent of temperature. The temperature dependent thermo-mechanical properties are shown in Table 2. The deposition of the weld bead during each pass was simulated using element deactivation and subsequent reactivation using ABAQUS. The details are explained in the section below. The inter-pass temperature between each weld pass was maintained at 50 °C. This was achieved by maintaining the sink temperature at the inter-pass temperature, so that no more heat loss occurred once the sample was cooled to 50 °C.

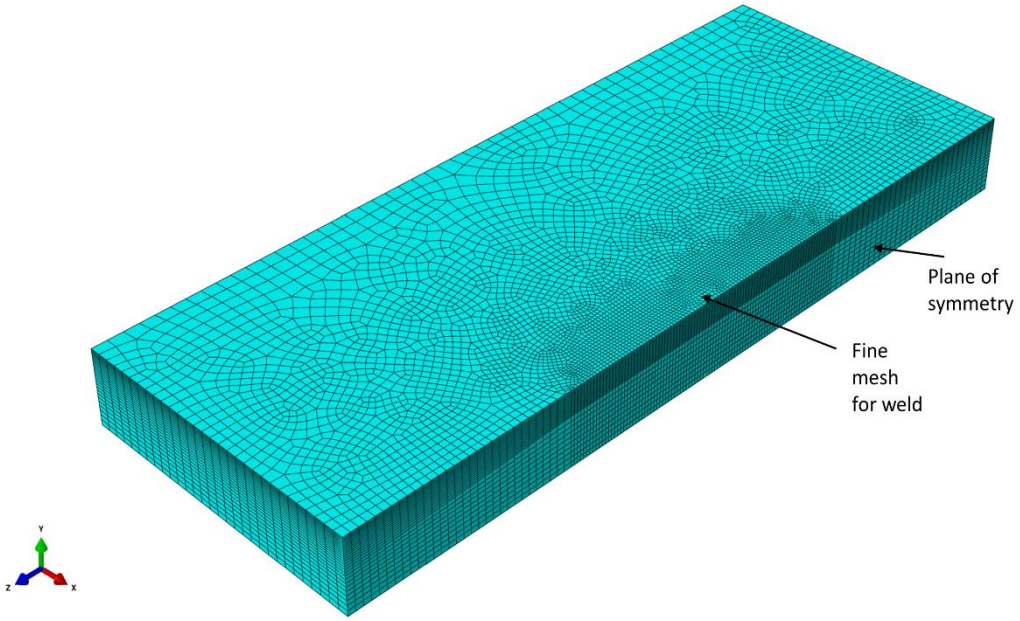

Fig. 7. Finite element mesh of the TG4 sample [7]

In order to model the deposition of the weld bead during each weld pass, in a multipass welding, ABAQUS functionality *Model Change was made use of in the thermal and the mechanical analysis [17]. To begin with, all the elements corresponding to each of the weld passes were modelled in the FEA model. Before the first weld pass was laid, the elements corresponding to the three weld passes were deactivated. Then the elements corresponding to the first weld pass were reactivated. Using the block dumping approach, the weld bead elements were heated, simulating the heating of the weld bead by the weld torch. After cooling down to the inter-pass temperature, the elements corresponding to the second weld pass were reactivated, before the volumetric heat flux was applied. The same was repeated for the elements corresponding to the third weld pass. The element deactivation and reactivation was modelled in both the thermal and mechanical analyses. The elements were reactivated with strain in the mechanical analysis.

The mechanical analysis was performed after the thermal analysis, with the results from the thermal analysis applied as predefined field. Temperature dependent material properties were used in the analysis. The model was constrained to avoid any rigid movement. Symmetry conditions were imposed on the plane of symmetry. Non-linearity in the geometry was considered in the analysis as a part of large displacement theory to take into account any changes in the geometry. A LeMaitre-Chaboche mixed hardening theory was used to model the hardening behaviour [18]. The combined components allow the Bauschinger effect and the cyclic hardening with plastic shakedown to be captured. Also, previous analysis by other researchers has shown that isotropic hardening exhibits a tendency to overpredict the residual stresses [2]. The parameters used for modelling mixed hardening are shown in Table 3. The annealing temperature was set as 1000 °C, at which the accumulated plastic strain history was set to zero. The residual stresses and strains were predicted as an output.

Table 2. Thermo-mechanical material properties of Type 316L base and weld material [16]

Temperature (°C)	Specific heat (kJ / kg °C)		Conductivity (W / m °C)	Thermal expansion coefficient x 10^{-6} ° C^{-1}	Young's Modulus (GPa)		Poisson's ratio	Density (kg/m^3)
	Parent	Weld			Parent	Weld		
20	0.492	0.488	14.12	14.56	195.6	171.0	0.294	7966
100	0.502	0.502	15.26	15.39	191.2	165.0		
200	0.514	0.520	16.69	16.21	185.7	157.5		
300	0.526	0.537	18.11	16.86	179.6	150.0		
400	0.538	0.555	19.54	17.37	172.6	142.5		
500	0.550	0.572	20.96	17.78	164.5	135.0		
600	0.562	0.589	22.38	18.12	155.0	127.5		
700	0.575	0.589	23.81	18.43	144.1	120.0		
800	0.587	0.589	25.23	18.72	131.4	109.0		
900	0.599	0.589	26.66	18.99	116.8	96.9		
1000	0.611	0.589	28.08	19.27	100.0	83.0		
1100	0.623	0.589	29.50	19.53	80.0	66.4		
1200	0.635	0.589	30.93	19.79	57.0	47.3		
1300	0.647	0.589	32.35	20.02	30.0	25.0		
1400	0.659	0.589	33.78	20.21	2.0	1.7		

Table 3. Chaboche parameters for mixed hardening for 316L stainless steel [2]

Temperature (°C)	$\sigma\|_0$ (MPa)	C_1 (MPa)	γ_1	C_2 (MPa)	γ_2	Q_{inf} (MPa)	b
20	125.6	156,435.00	1410.85	6134.00	47.19	153.4	6.9
275	97.6	100,631.00	1410.85	5568.00	47.19	154.7	6.9
550	90.9	64,631.00	1410.85	5227.00	47.19	150.6	6.9
750	71.4	56,232.00	1410.85	4108.00	47.19	57.9	6.9
900	66.2	0.05	1410.85	292.00	47.19	0	6.9
1000	31.82	0	1410.85	0	47.19	0	6.9
1100	19.73	0	1410.85	0	47.19	0	6.9
1400	2.1	0	1410.85	0	47.19	0	6.9

7. Results and Discussion

7.1 Deep-hole drilling measurement results

The longitudinal (zz), transverse (xx) and the in-plane shear residual stresses (zx) measured through the thickness of the sample (line BD) using incremental deep-hole drilling are shown in Fig. 8. It can be seen from the graph that the longitudinal (zz) and transverse (yy) stresses follow a similar trend with differing magnitudes. The shear component (zx) is negligible as expected due to the symmetry conditions. Comparing with the results from the measurements through the thickness conducted on SALSA shown in Fig.12, it can be seen that the incremental method has successfully captured the residual stress profile avoiding any effects from the release of plasticity during trepanning [6].

7.2 Neutron diffraction results

The residual stress profile along the line BD measured on strain diffractometer E3 is shown in Fig.9. From the residual stress, it is observed that the normal stress (yy) is very small in magnitude especially closer to the top and bottom surfaces of the plate, which is expected and can be used as a validation for the FE analysis. Further comparing the stress profile with those from Fig. 8, it is clear that the stress magnitude closer to the surface is matched very well. However, at mid-thickness the stresses are relatively higher. The measurements along the line D2 and B2 on the strain diffractometer E3 are shown in Fig. 10 and 11 respectively. Fig. 12, 13, 14 and 15 indicate the residual stress profiles through the lines BD, repeat measurement along the line BD, D2 and B2 on the strain diffractometer SALSA.

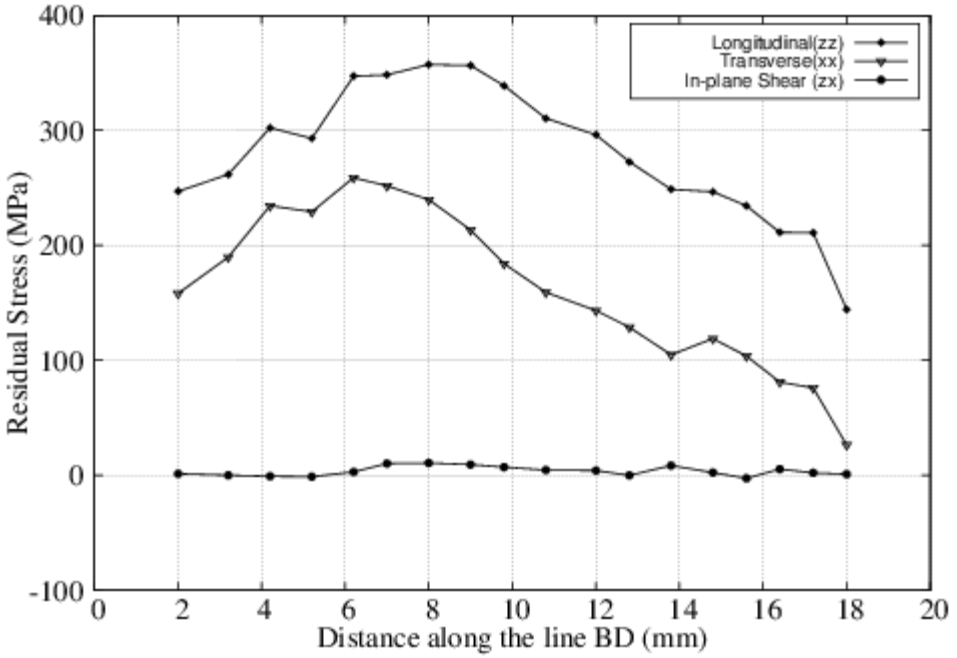

Fig. 8. Residual stress profile through line BD from weld top and bottom surface of the plate from incremental deep-hole drilling measurements

The residual stress along the line BD from the measurements on strain diffractometer E3 indicate that the longitudinal residual stress is higher in magnitude on the specimen than that from the measurements on strain diffractometer SALSA. This could be attributed to the fact that the measurements were made on two samples manufactured using different welding procedures. However, the trend remains the same with high tensile stresses at a depth of ~ 7mm from the top both in longitudinal (zz) as well as transverse (xx) directions. The magnitude of normal stress (yy) is negligible on the measurements from E3. The measurements from strain diffractometer SALSA on line BD from Fig.12, indicate a normal stress (yy) of ~ 100MPa, however this could be cancelled from the scatter/error in the measurement (~ 70MPa). Nevertheless, comparing the repeat measurements on the line BD from strain diffractometer SALSA, i.e., Fig. 12 and Fig. 13, it can be seen that the profiles are completely different. No possible explanation could be derived for these variations except instrumentation and measurement associated errors. Consideration should be given to the fact that in Fig. 12 the longitudinal (zz) and transverse (xx) residual profiles are in good agreement with those from Fig. 8 and Fig. 9. In any case, a repeat measurement is suggested to provide a better explanation for this abnormality in the normal stress (yy) profile.

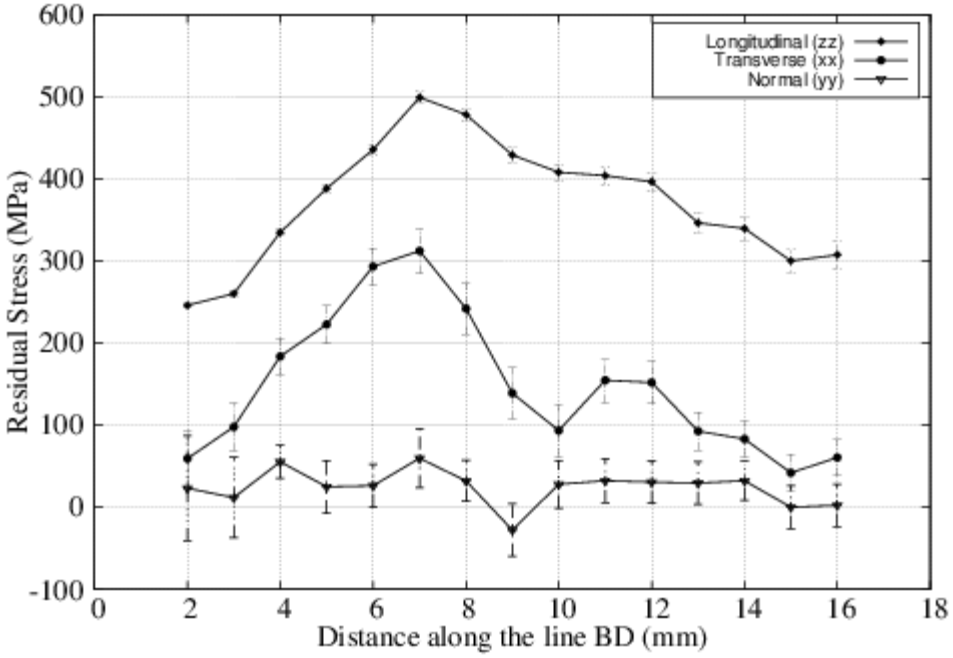

Fig. 9. Residual stress profile through the line BD from weld top to the bottom surface of the plate using neutron diffraction on strain diffractometer E3

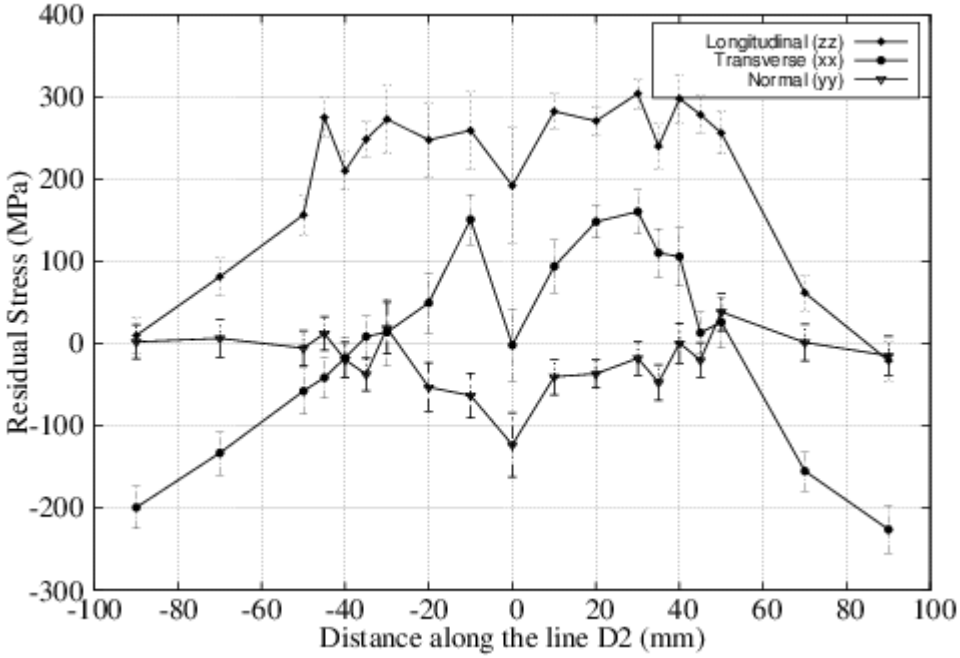

Fig. 10. Residual stress profile along the line D2 in welding direction using neutron diffraction on strain diffractometer E3

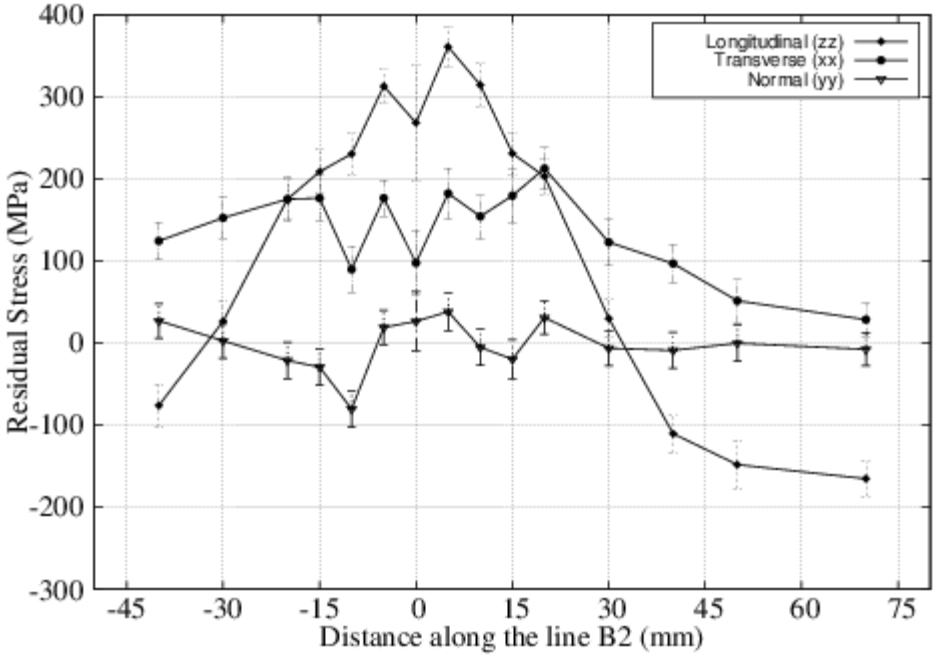

Fig. 11. Residual stress profile along the line B2 using neutron diffraction on strain diffractometer E3

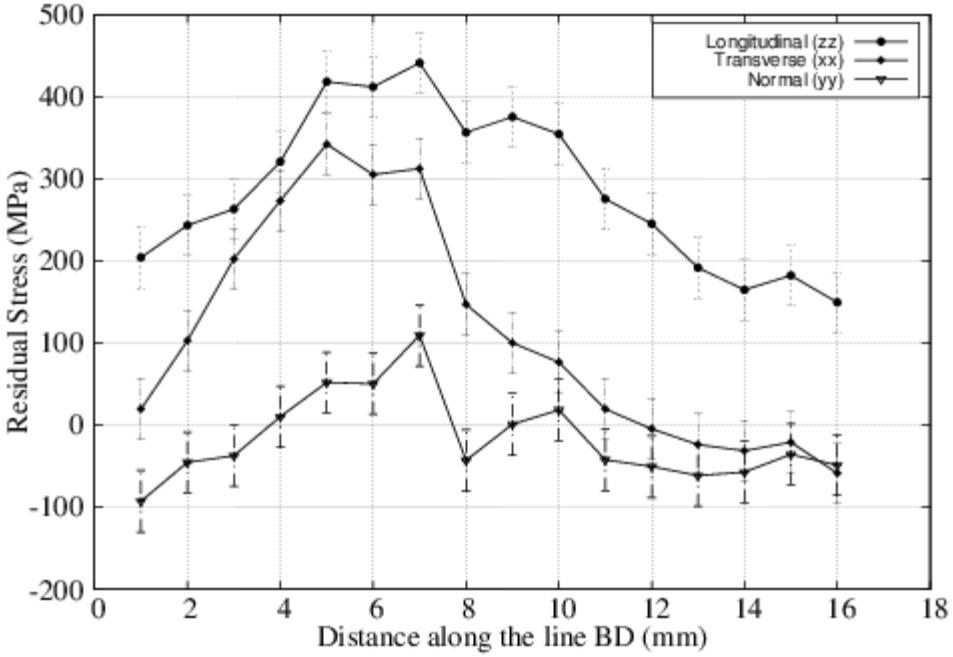

Fig. 12. Residual stress profile through the line BD from weld top to the bottom surface of the plate using neutron diffraction on strain diffractometer SALSA

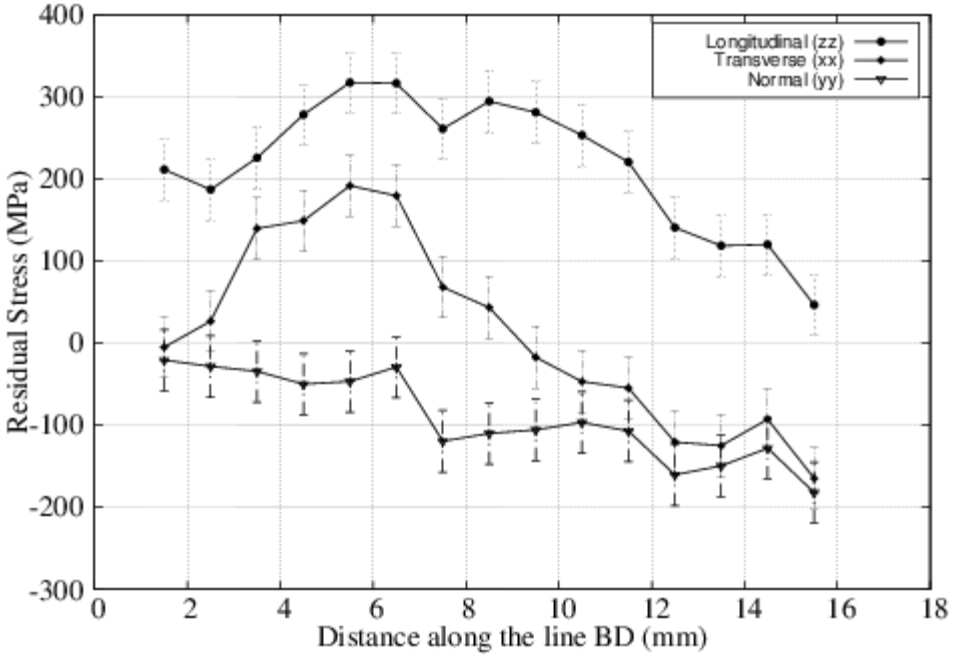

Fig. 13. Residual stress profile through the line BD from weld top to the bottom surface of the plate using repeat neutron diffraction on strain diffractometer SALSA at 180°

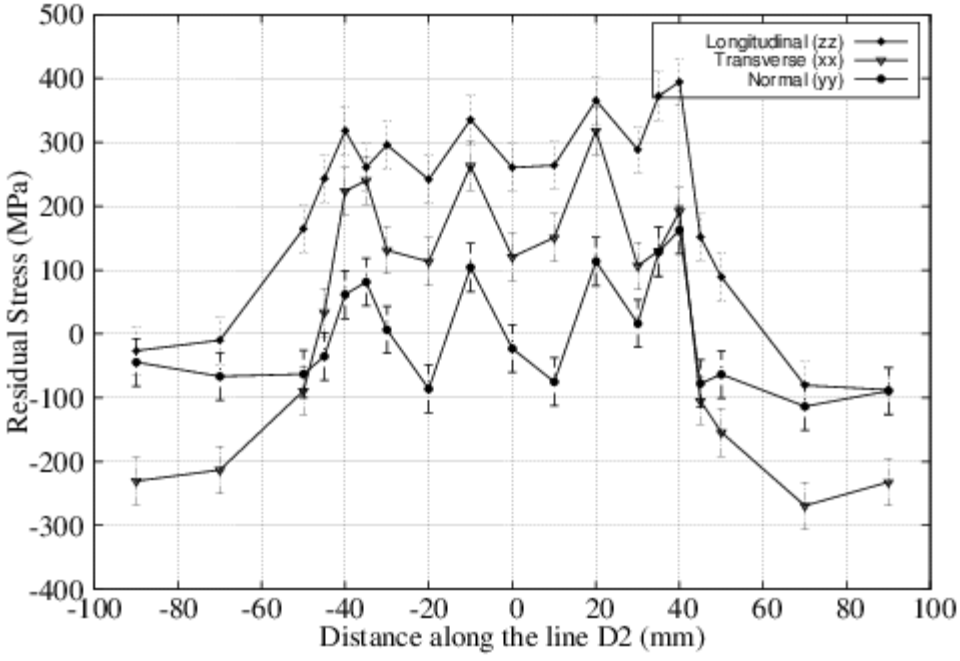

Fig. 14. Residual stress profile along the line D2 in the welding direction using neutron diffraction on strain diffractometer SALSA

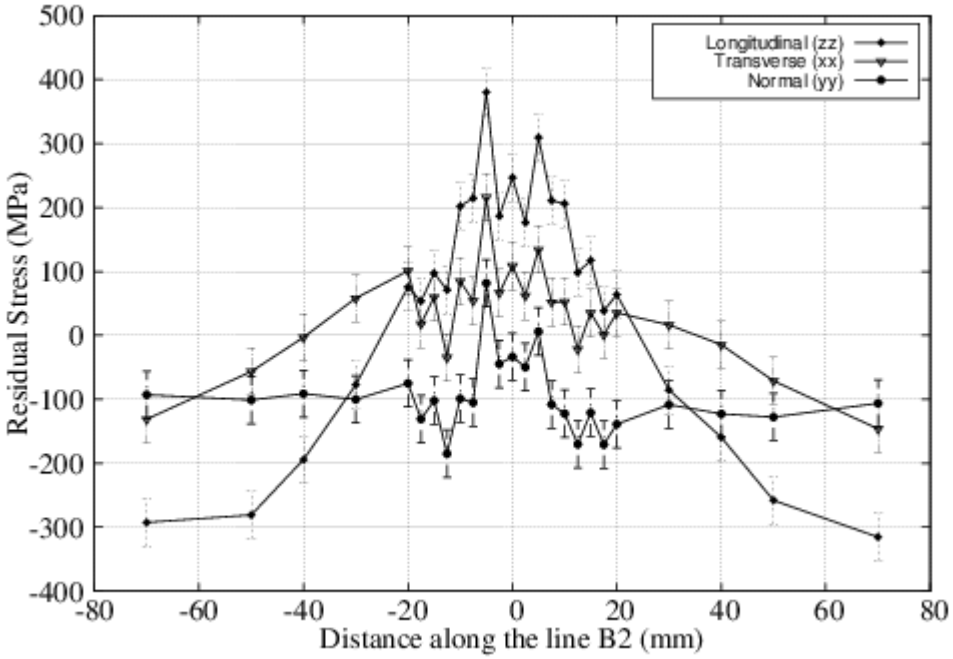

Fig. 15. Residual stress profile along the line B2 using neutron diffraction on strain diffractometer SALSA

7.3 Finite element analysis results

The predictions from the FE analysis of a three-pass weld in an austenitic plate are presented in this section. The cross-sectional weld macrograph measured by sectioning the specimen is shown in Fig. 16. The weld fusion zone predicted by the thermal isotherm 1400 °C for each of the three passes is shown in Fig. 17. The weld fusion zone was determined from element collection which had attained 1400 °C and above during the deposition of the weld bead. The predicted weld fusion boundary for the TG4 model when compared with the cross-weld macrograph shown in Fig.16 agrees satisfactorily. A comparison of the temperature vs. time predictions at the thermocouple location TC9 at the centre of the plate on the bottom surface, TC9, with those from the thermocouple recordings [3] are presented in Fig. 18. It is noticed that the predicted thermal history compares well with the recorded values indicating that the thermal analysis is accurate. In order to further validate the thermal profiles based on the root mean square error proposed in TG1 problem, the mean measured temperature increase for thermocouple TC9 was calculated based on the recordings for all the specimens from batch one. The root mean square error was calculated for each weld pass using Eq. (13) based on thermocouple TC9 [19].

$$ERROR_{RMS} = \sqrt{\left(\frac{\Delta TC9_{Predicted} - \Delta TC9_{mean}}{\Delta TC9_{mean}}\right)^2} \quad (13)$$

where $\Delta TC9_{Predicted}$ is the peak predicted temperature rise, $\Delta TC9_{mean}$ is the mean measured increase. It is observed that the $ERROR_{RMS}$ is less than 10% for each pass.

The residual stress profiles are presented along the lines D2, B2 and BD explained in Fig. 5. The stress profile predicted along the line D2 is shown in Fig. 19. The stress profile along the lines B2 and BD are shown in Fig. 20 and Fig. 21 respectively. The start and stop end effects cannot be seen in the longitudinal (zz) and the transverse (xx) stress profile in Fig.19. This is because block-dumped analysis fails to capture these effects, whereas a moving heat source can adequately predict these effects, thereby incorporating them in the subsequent mechanical analysis. The normal component (yy) has relatively insignificant stress level. This is expected in a conventional welding processes, where the heat intensity is quite low and thereby the heat dissipation to the surrounding region in the transverse (xx) direction is proportionately greater compared to the normal (yy) direction. Hence the normal component (yy) which lies out of plane to welding direction, has insignificant stresses (~ 20MPa). The transverse component (xx) is qualitatively similar to the longitudinal component (zz) but differs in magnitude. At the far ends, the stress values drop to zero.

The measured longitudinal residual stress (zz) along line BD is plotted against the predicted value in Fig. 22. The graph indicates that the predictions are in agreement with iDHD measurements, albeit some discrepancy. The

measured and predicted longitudinal residual stress (zz) profile along line B2 are displayed in Fig. 23. From the plot, it is evident that the profile matches closely between measurements and predictions. Furthermore, it can be clearly seen that the predictions are consistent with measurements from strain diffractometer E3. The chart linking the longitudinal stress profiles (zz) along line D2 from simulation and experiments is shown in Fig. 24. It is apparent that a good correlation exists between the predictions and measurements. Based on the data, it can be concluded that although block-dumped analysis cannot predict the exact thermal gradients in the local areas of the weld region such as weld start and weld stop, the global thermal distribution through-out the sample can be predicted with reasonable accuracy and can be used for reliable residual stress prediction.

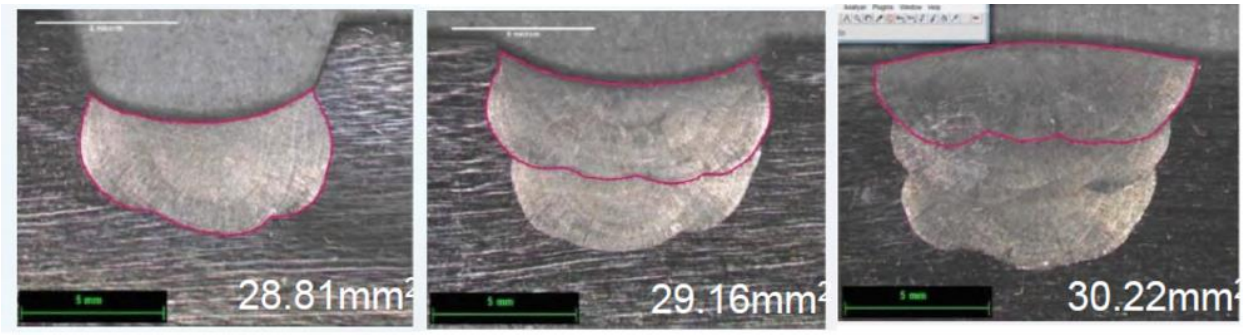

Fig. 16. Cross-sectional weld macrograph of the TG4 specimen [3]

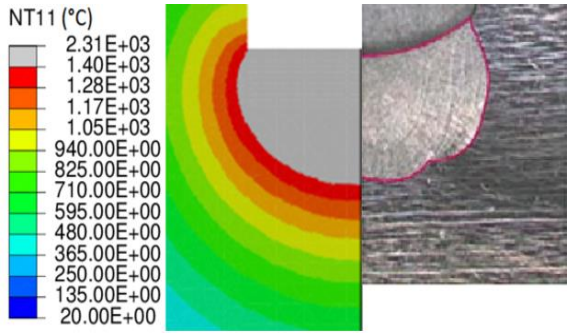

(a) Weld fusion boundary for pass 1

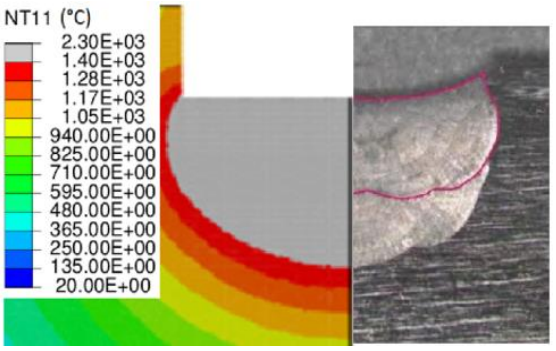

(b) Weld fusion boundary for pass 2

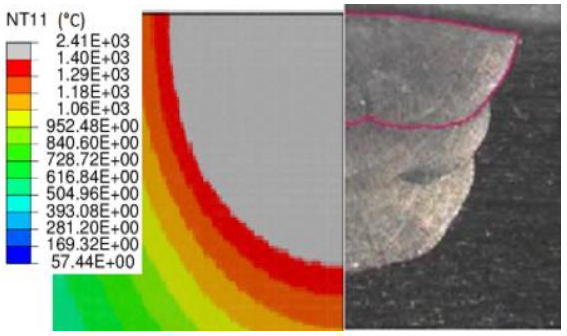

(c) Weld fusion boundary for pass 3

Fig. 17. Predicted weld fusion boundary for NeT TG4 model

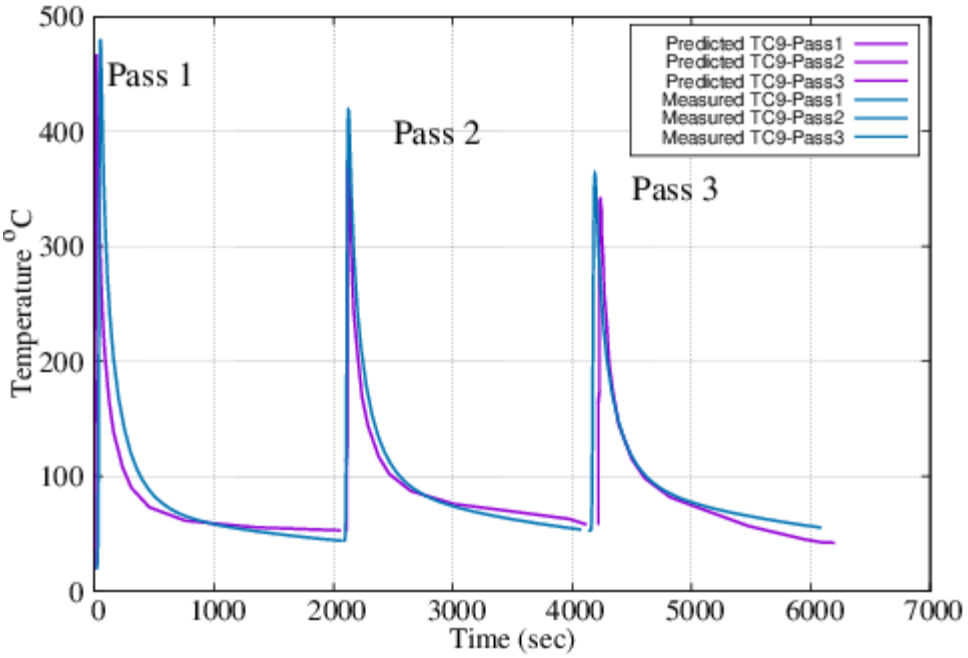

Fig. 18. Comparison of predicted and recorded temperature measurements on TG4 sample for thermocouple TC9

Finally, the predicted longitudinal residual stress (zz) along line D2 from the current model presented above is compared with those published by other participants [2] as a part of the round robin study of FE modelling and predictions. From the graph presented in Fig. 25, it is apparent that the residual stress profiles match very closely with each other. However, there is an apparent difference in the profiles at the weld stop location. This can be attributed to the differences in the weld bead shape of the FE models and the heat source employed. The authors from [2] used an advanced moving heat source for thermal model that can capture the transient thermal effects accurately than a block-dumped source. Despite these variations, there is a very good agreement with the predictions from both the models.

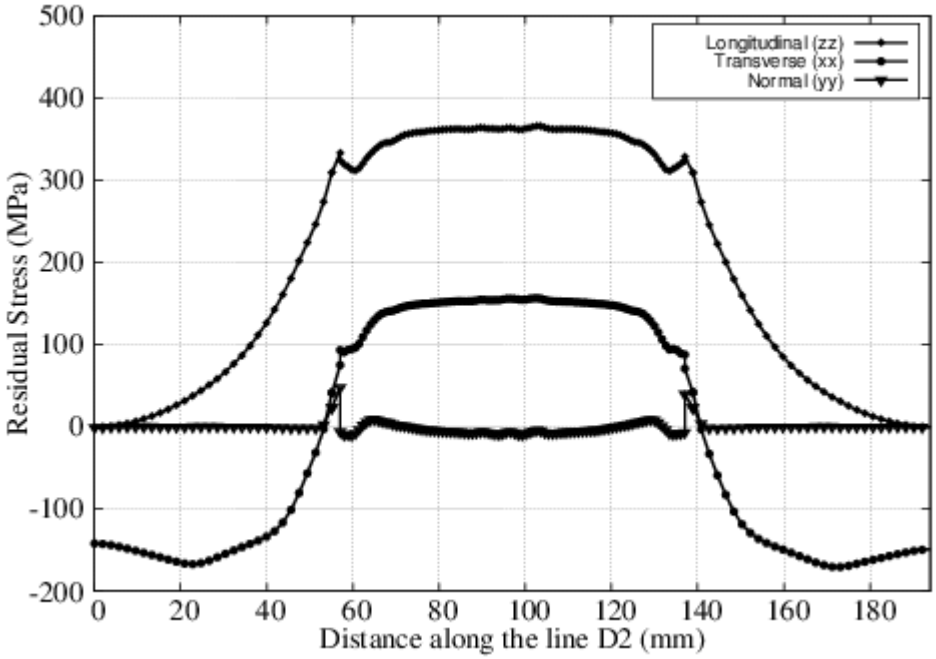

Fig. 19. Predicted residual stress along line D2 in the welding direction

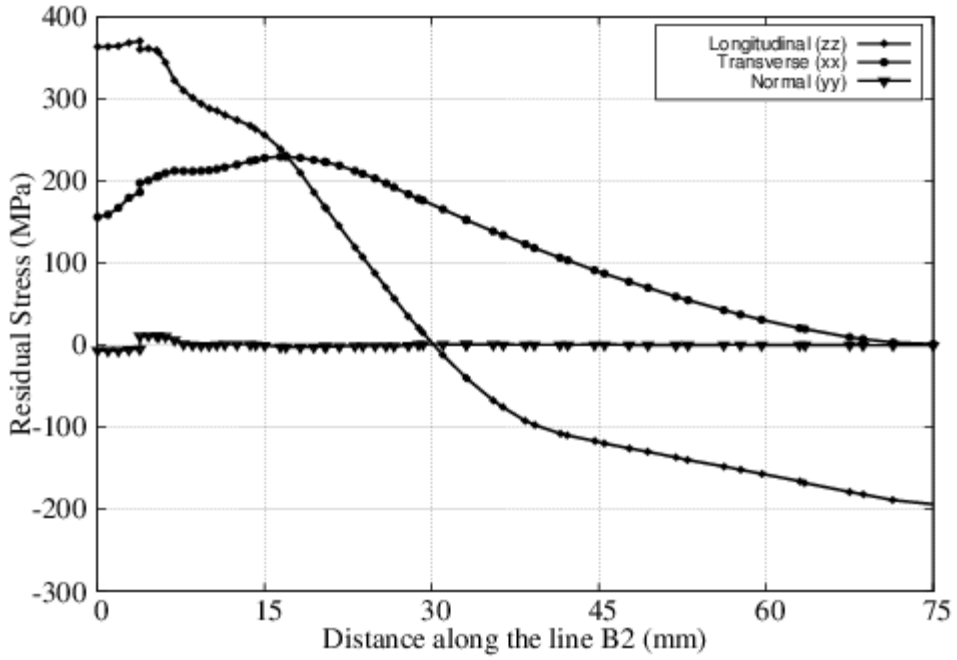

Fig. 20. Prediction residual stress along line B2 from weld centre to the parent material

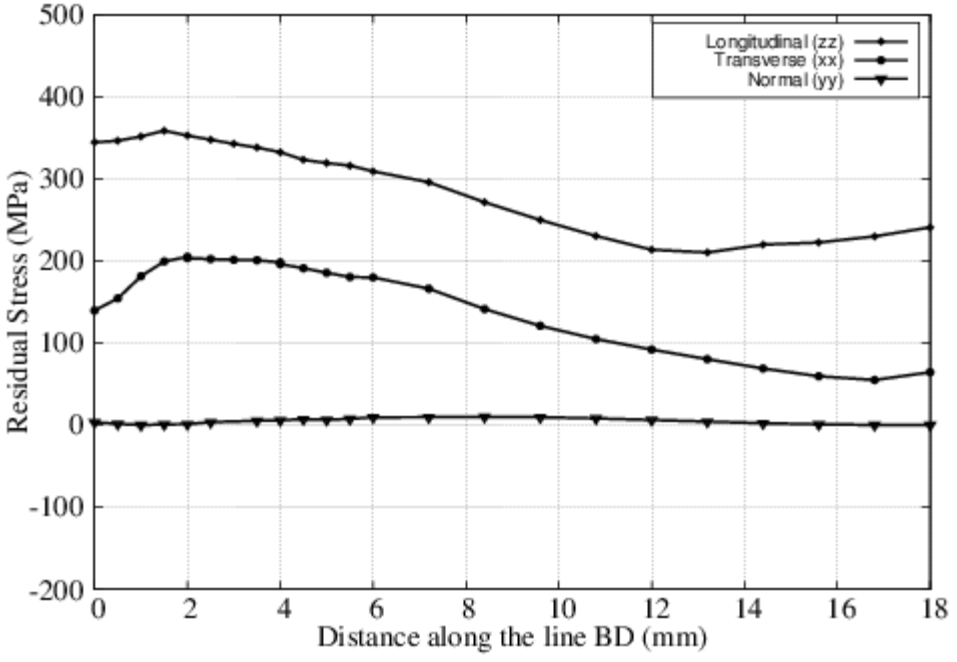

Fig. 21. Prediction residual stress along line BD from weld top to the bottom surface of the plate

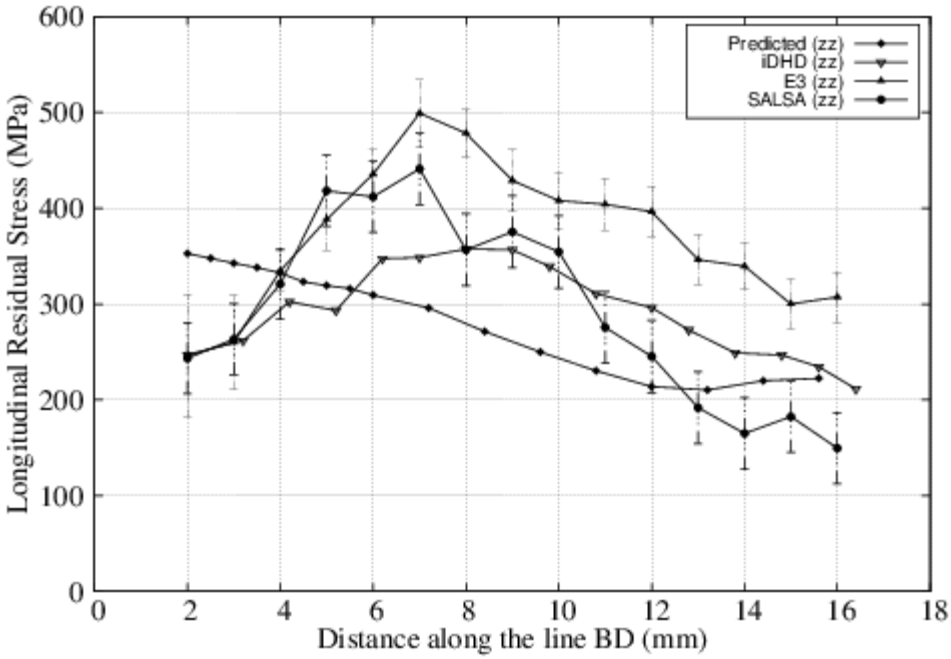

Fig. 22. Comparison of longitudinal residual stress from prediction and measurement along line BD from weld top to the bottom surface of the plate

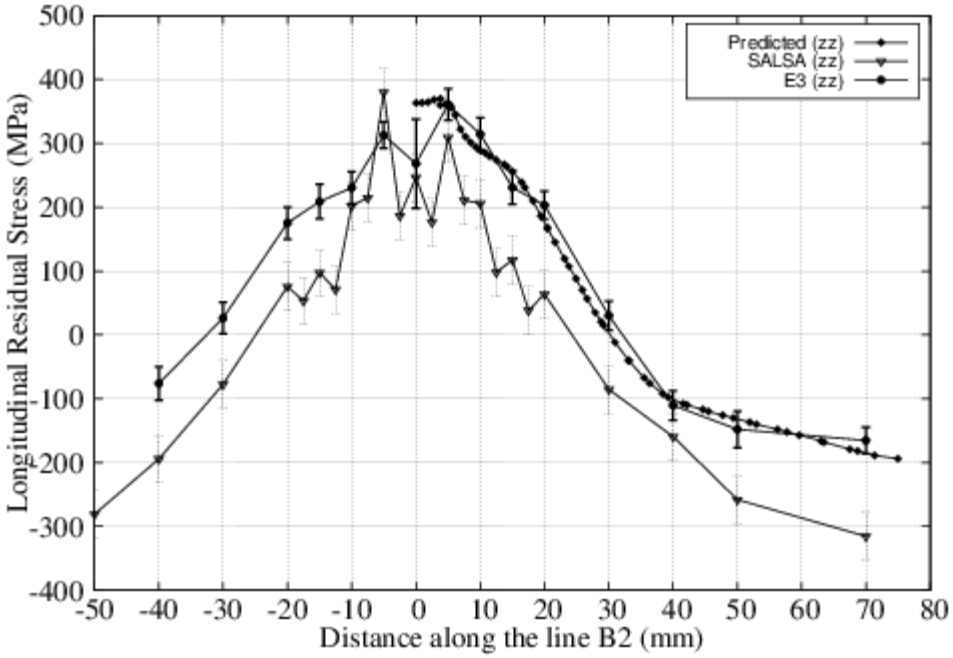

Fig. 23. Comparison of longitudinal residual stress from prediction and measurement along line B2

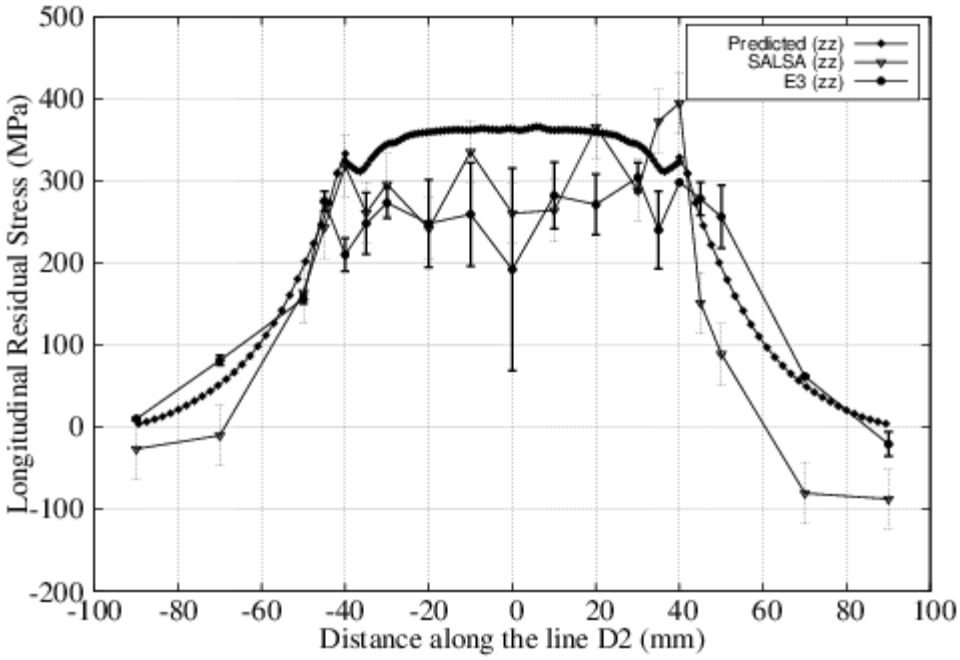

Fig. 24. Comparison of longitudinal residual stress from prediction and measurement along line D2 along welding direction

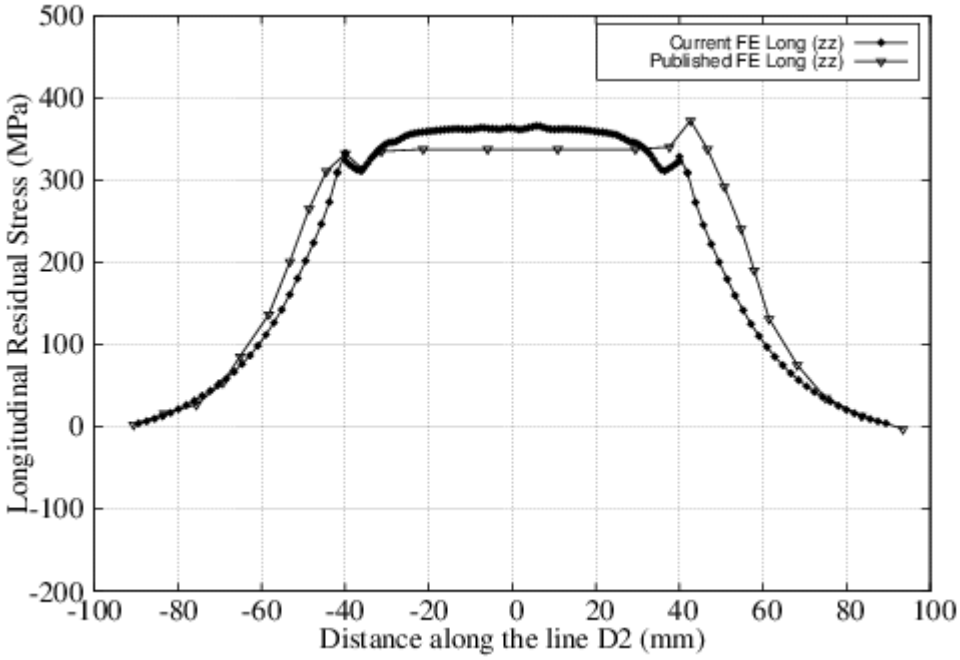

Fig. 25. Comparison of longitudinal residual stress along line D2 with published results from other round robin partners [2]

8. Conclusions

Based on the various experiments and finite element analysis on a three-pass slot welded austenitic 316LN stainless steel plates using TIG welding, the following conclusions can be drawn;

1. Incremental deep-hole drilling has been successfully employed to measure the residual stress profile in regions influenced by high plastic strains arising from manufacturing processes such as welding.
2. For accurate estimation of residual stresses, it is recommended to characterise the stresses through two or more independent measurement techniques.
3. The reason for the variation in residual stress profile through the thickness, between the original and repeat measurement on SALSA at ILL, is inconclusive and needs to be investigated further using a repeat measurement.
4. Block-dumping technique can identify the peak temperatures with acceptable accuracy in the regions under steady-state conditions during the welding process and thereby predict the residual stresses reasonably well in these regions.
5. A good agreement is observed in general between the measured residual stress profiles with those from predictions, indicating that the transient thermal predictions from the model are in close match with those from the actual welding process.
6. Although block-dumped heat source model suffers from lower accuracy compared to that of moving heat source, the residual stress profile can still be predicted accurately provided the transient peak temperatures are predicted accurately.

References

[1] Smith M, Smith A, "NeT Task Group 4: Three-pass slot weld specimen in austentitc stainless steel: NeT TG4 manufacturing history", Technical report, NeT-TG4 Steering Group, 2009.

[2] Muransky O, Hamelin CJ, Smith MC, Bendeich PJ, Edwards L. The effect of plasticity theory on predicted residual stress fields in numerical weld analyses. Comp. Mater. Sci. 2012;54:125 – 134.

[3] Muransky O, Smith MC, Beindeich PJ, Holden TM, Luzen V, Martins RV, Edwards L. Comprehensive numerical analysis of three-pass bead-in-slot and its critical validation using neutron and synchrotron diffraction residual stress measurements. Int. J. Solids Struct. 2012;49(9): 1045 – 1062.

[4] Francis JA, Smith M, Smith A. The manufacuting of a three-pass slot weld specimen in AISI Grade 316L Austenitic Stainless Steel. Technical Report, NeT TG4 Steering Group, 2009.

[5] Kingston E, Smith DJ, Zheng G, Gill C, Hurell P, Measurement of residual stresses in thick section steel electron beam welds. Proc. Int. Pres. Ves. Pip – ASME 2010;PVP2010-25314: 1307 - 1316.

[6] Mahmoudi AH, Pavier MJ, Truman CE, Smith DJ. Accurate measurement of highly triaxial residual stresses. Soc. Exp. Mech. Conf. 2007;

[7] Abburi Venkata K. Characterising high energy beam welding in structural steels with numerical simulation and validation. 2015. PhD Thesis. Department of Mechanical Engineering. University of Bristol.

[8] Hossain S, Truman CE, Smith DJ. Finite element validation of the deep-hole drilling method for measuring residual stresses. Int. J. Pres. Ves. Pip. 2012;93-94: 29 – 41.

[9] Lambda Technologies. Measurement of Residual Stresses using Ring-Core Technique. Diffraction Notes. 2005:31.

[10] Hutchings MT, Withers PJ, Holden TM, Lorentzen T. Introduction to the characterisation of residual stress by neutron diffraction. CRC Press. 2005.

[11] Smith DJ, Bouchard PJ. George D. Measurement and prediction of residual stresses in thick-section steel welds. J. Strain. Anal. 2000;35(4): 287 - 305.

[12] Withers PJ, Preuss M, Steuwerb A, Pang JWL. Methods for obtaining strain-free lattice parameter when using diffraction to determine residual stresses. J. Appl. Cryst. 2007;40: 891 – 904.

[13] Webster PJ. The Neutron Strain Scanner: Measurements in Welds. In: Mechanical Effects of Welding. Int. U. Theo. Appl. Mech. 1992.

[14] Lodini A. Calculation of residual stress from measured strain. In: Lodini A, Fitzpatrick ME (Eds.) Analysis of residual stress using neutron and synchrotron radiation. London: Taylor & Francis 2003; 47 – 59.

[15] Elcoate CD, Bouchard PJ, Smith MC. 3-Dimensional Repair Weld Simulations – Bead on Plate Comparisons. In: host publication. ABAQUS User Group Conf. 2003.

[16] Shan X, Davies CM, Wangsdan T, O'Dowd NP, Nikbin KM. Thermo-mechanical modelling of a single-bead-on-plate weld using finite element method. Int. J. Pres. Ves. Pip. 2009;86(1): 110 – 121.

[17] Lindgren LE, Finite Element Modelling and Simulation of Welding Part I: Increased Complexity. J. Thermal Stresses. 2001;24(2): 141 – 192.

[18] Lemaitre J, Chaboche J-L. Mechanics of Solid Materials. 1990 Cambridge University Press.
[19] Bouchard PJ. The NeT bead-on-plate benchmark for weld residual stress simulation. Int. J. Pres. Ves. Pip. 2009;86(1): 31 – 42.